Atmos. Chem. Phys. Discuss., 14, 2087–2111, 2014
www.atmos-chem-phys-discuss.net/14/2087/2014/
doi:10.5194/acpd-14-2087-2014

Atmospheric Chemistry and Physics Discussions

Composition of 15–80 nm particles in marine air

M. J. Lawler[1,2], **J. Whitehead**[4], **C. O'Dowd**[5], **C. Monahan**[5], **G. McFiggans**[4], **and J. N. Smith**[1,2,3]

[1]Atmospheric Chemistry Division, National Center for Atmospheric Research, Boulder, USA
[2]Department of Applied Physics, University of Eastern Finland, Kuopio, Finland
[3]Finnish Meteorological Institute, Kuopio, Finland
[4]Centre for Atmospheric Science, University of Manchester, UK
[5]Centre for Climate & Air Pollution Studies, National University of Ireland, Galway, Ireland

Received: 15 November 2013 – Accepted: 5 January 2014 – Published: 23 January 2014

Correspondence to: M. J. Lawler (mlawler@ucar.edu)

Published by Copernicus Publications on behalf of the European Geosciences Union.

Abstract

The chemical composition of 15–80 nm diameter particles was measured at Mace Head, Ireland, during May 2011 using the TDCIMS (Thermal Desorption Chemical Ionization Mass Spectrometer). Measurable levels of chloride, sodium, and sulfate were present in essentially all collected samples of these particles at this coastal Atlantic site. Organic compounds were rarely detectable, but this was likely an instrumental limitation. Concomitant particle hygroscopicity observations usually showed two main modes, one which contained a large sea salt component and another which was likely dominated by sulfate. There were several occasions lasting from hours to about two days during which 10–60 nm particle number increased dramatically in polar oceanic air. During these events, the sulfate mode increased substantially in number. This observation, along with the presence of very small (<10 nm) particles during the events, suggests that the particles were formed by homogeneous nucleation, followed by subsequent growth by sulfuric acid and potentially other vapors. The frequency of the events and similarity of event particles to background particles suggest that these events are important contributors of nanoparticles in this environment.

1 Introduction

Particles in the atmosphere play important roles in the global climate through direct interaction with radiation and by becoming cloud condensation nuclei (CCN), which influence the formation and properties of clouds. Understanding controls on cloud extent and type is critical for predicting future climate (Solomon et al., 2007). The formation and growth of particles from gas phase species in the atmosphere is likely a significant contributor to aerosol number and atmospheric optical depth in a variety of environments, and this process may therefore influence CCN concentrations (Kulmala et al., 2004; Wang and Penner, 2009; Yu and Luo, 2009; Spracklen et al., 2006). Water vapor uptake on small, recently formed particles is limited by the Kelvin effect, so new parti-

ACPD
14, 2087–2111, 2014

cles must grow via uptake of other species before they are large enough to act as CCN. In the marine boundary layer, where cloud water vapor supersaturations are typically around 0.2 %, even very hygroscopic sea salt aerosols must be greater than 70 nm in diameter before they are activated into cloud droplets (Hoppel et al., 1996; Seinfeld and Pandis, 1997). For this reason, in order for homogeneously nucleated particles to have a significant impact on cloud formation, they must grow swiftly enough to CCN size before they are lost by coagulation onto existing aerosol. Condensation of low volatility vapors and/or multiphase reactive uptake are required to accomplish this growth (Khvorostyanov and Curry, 2007; Donahue et al., 2011).

Many different compounds are involved in particle nucleation and growth, and different compounds are likely important under different conditions. Sulfuric acid (H_2SO_4) may be critical for particle nucleation throughout the atmosphere, and it has been shown to contribute to nanoparticle growth (Kuang et al., 2008; Eisele and McMurry, 1997; Bzdek et al., 2012). However, beyond the very initial stages of particle formation, H_2SO_4 probably plays a small role in the boundary layer (Kuang et al., 2012, 2008; Zhang et al., 2012). For particle diameters larger than ~ 10 nm in diameter, observations from a variety of environments suggest that condensation of organic vapors contribute greatly to particle growth (Kuang et al., 2012; Bzdek et al., 2011; Donahue et al., 2011). Multifunctional acidic organic species are thought to be likely contributors to particle growth due to their low vapor pressures (Zhang et al., 2012). Recently nucleated particles have been observed in coastal regions that experience large sea–air fluxes of readily photolyzable iodine-containing species (O'Dowd and Hoffmann, 2005; Mäkelä, 2002; Whitehead et al., 2009, 2010; McFiggans et al., 2010).

The particle distribution in the Marine Boundary Layer (MBL) is an important climate parameter. The MBL is characterized by relatively low particle concentrations compared to the terrrestrial boundary layer (Heintzenberg et al., 2000; Spracklen et al., 2010). Small changes in particle number are therefore more likely to have an effect on ensemble aerosol properties and CCN numbers, and newly formed particles have more time to grow to CCN size before coagulation. For example, Pierce and Adams

ACPD
14, 2087–2111, 2014

(2006) showed that the inclusion of small sea salt aerosols in a general circulation model increased the CCN concentrations in some regions as much as 500 %. Also, cloud albedo is in general significantly higher than ocean albedo, making the relative per-area radiative impacts of cloud formation high. An understanding of how CCN are formed in the MBL is necessary for good parameterizations of cloud formation over the global oceans.

Sub-micron MBL particles are typically found in two dominant modes: an accumulation mode centered around 150 nm diameter, and an Aitken mode centered around 50 nm diameter (Heintzenberg et al., 2000). Particles at intermediate sizes tend to grow quickly to larger sizes. Smaller particles either quickly grow, are accommodated onto existing aerosol, or are deposited to the sea surface, depending on the availability of condensable vapors and the aerosol size distribution (McMurry, 1983). Sea salt is typically the primary component of super-micron MBL aerosol, but smaller MBL particles likely contain significant fractions of sulfate and organics (Mcinnes et al., 1997; Allan, 2004). Nonetheless, recent lab and in situ studies show that bubble bursting at the ocean surface can generate large numbers of sub-100 nm particles, raising the possibility that the MBL Aitken mode has a large sea salt aerosol component (Clarke et al., 2006; Russell and Singh, 2006). Clarke et al. (2003) showed that wave breaking contributed significantly to sub-100 nm particles measured at a coastal site, with a peak in the number distribution at $\sim$ 30 nm. Observations at Mace Head, Ireland, show evidence for apparent "open ocean particle production" characterized by enhancements in particle number in the 15–50 nm diameter range as well as slow growth rates of the order of 0.8 nm h^{-1} (Dall'Osto et al., 2011; O'Dowd et al., 2010). Total number concentrations during these conditions are on average about 8× larger than for background conditions (Dall'Osto et al., 2011).

We present measurements of nanoparticle chemical composition and hygroscopicity made in marine air at Mace Head during May 2011. These observations provide insights into the formation and growth of small marine particles, with implications for the role of new particle formation in marine atmospheric chemistry and climate.

ACPD
14, 2087–2111, 2014

2 Site and methods

2.1 Mace Head

The Mace Head Atmospheric Research Station is located on the west coast of Ireland at 53°20′ N, 9°54′ W. Measurements of the molecular composition of marine nanoparticles were made between 14–31 May 2011, during the Marine Aerosol–Cloud Interactions (MaCloud Inc.) campaign. During this period, the air temperature ranged from 7.6–13.4 °C, with a mean of 11.0 °C and typical diel range of 2–3 °C. The relative humidity ranged from 56–98 %, with a mean of 82 ± 10 % (1 std dev). Winds were consistently onshore and typically W to SW, and they ranged from 3.1–25.2 $m s^{-1}$, with a mean of 10.9 ± 3.1 $m s^{-1}$ (1 std dev). Air mass back trajectories were calculated for air arriving at the site using the NAME III dispersion model (UK Met Office) and the HYSPLIT model (NOAA) (Draxler and Hess, 1997). The air masses arriving at the site originated in polar regions, North America, and the subtropics, but rarely if at all from continental Europe.

Particle size distributions were measured using an Scanning Mobility Particle Sizer (SMPS), consisting of a long differential mobility analyzer (model 3081; TSI, Inc.) and condensation particle counter (model 3010; TSI, Inc.). SMPS measurements were performed continuously with a roughly 3 min time resolution.

2.2 TDCIMS instrument

Particle chemical composition was measured using the Thermal Desorption Chemical Ionization Mass Spectrometer (TDCIMS). This instrument has been described in detail elsewhere (Smith et al., 2004; Voisin et al., 2003). The instrument draws ambient air through a pair of unipolar chargers (UPCs), where small particles are efficiently charged by ion diffusion (Chen and Pui, 1999). The particles are size selected in radial differential mobility analyzers, or RDMAs (Zhang et al., 1995), operating at low resolution (McMurry et al., 2009). Particle mobilities corresponding to singly charged

ACPD
14, 2087–2111, 2014

particles of 15, 20, or 30 nm diameter are selected for analysis based on ambient aerosol size distributions. Charged, size-selected aerosols are electrostatically precipitated onto a loop of Pt wire maintained at 4000 V relative to ground for a sampling time of typically 30 min. The wire is shielded from contamination from neutral aerosols and gases by a sheath of clean N_2. After the collection period, the wire is translated into an ion source region containing an ^{241}Am alpha-emitting radioactive foil. Here the wire is heated by a 70 s programmed current ramp from room temperature to ~ 600 °C to desorb the compounds contained in the collected aerosol. The reagent ions generated by the ion source react with desorbed compounds from the collected aerosol to form product ions, which are passed through a collisional dissociation chamber and an ocotopole ion guide before being detected with a mass spectrometer.

The TDCIMS is capable of observing ions of both polarities, but only one polarity for a given sample. At all times, the ion source is filled with ultra high purity N_2 gas. The reagent ions are provided by small impurities in the N_2. In negative ion mode, the reagent ions are O_2^- and $(H_2O)_nO_2^-$ clusters. This chemistry is particularly effective for generating ions from strong gas-phase acids (both organic and inorganic) (Smith and Rathbone, 2008). In positive ion mode, the reagent ions are H_3O^+ and larger water clusters. Ammonia, amines, and some oxygenated hydrocarbons can be ionized by this chemistry.

The instrument was operated on a roughly 2 h cycle including aerosol collection and a "background" for both positive and negative ions. The background signal is assessed using the same procedures as the collection, but without applying a collection voltage to the wire. The background signal therefore represents the accumulation of neutral gases and/or particles on the wire, due either to diffusion of gases from nearby instrument surfaces or to some of the sample air mixing into the N_2 sheath gas flowing past the wire, as well as the contribution by any semi-volatile species that desorb from the walls of the ion source while the collection wire is heated during analysis. Both collection and background signals represent integrated "desorption period" ion counts, which have a pre-desorption baseline signal removed. These signals are scaled at ev-

ACPD
14, 2087–2111, 2014

ery point by reagent ion signal to account for changes in sensitivity arising due to slight changes in the reagent ion concentration. The reported aerosol composition measurements here have had the background signal subtracted. Signal errors were estimated as the square root of counted ions, and errors were propagated for all arithmetic operations. Detectable signal was defined as background-corrected signals which were two standard errors above zero.

The TDCIMS signals are reported here as fractions of total detectable ion signal for each collected mass spectrum. This was done, rather than using absolute ion signal or collected mass- or volume-normalized ion signal, to avoid uncertainties and potentially misleading interpretations stemming from the variability in particle volume and sizes collected. Estimated uncertainties in the collected mass are significant, usually on the order of 50 % but sometimes higher. This is primarily due to the effects of multiple charging in the unipolar chargers (McMurry et al., 2009). A water-based condensation particle counter (CPC; model 3787; TSI Inc.) was located downstream of the TDCIMS collection wire. This allowed for an accurate assessment of number collected, by comparing sampling and background particle concentrations. To estimate the particle volume collected, it was necessary to estimate the actual size distribution of collected particles. This depends on the ambient distribution, the selected electrical mobility, the size-dependent transmission and collection efficiency, and the distribution of charge number for a given particle size. The collected volume estimation was done using laboratory observations of multiple charging and transmission in the system, alongside an inverse model that optimized an empirical sampling efficiency function to match observed ambient particle size distributions to the TDCIMS CPC number concentrations. The approximate maximum sizes of collected particles for nominal 15, 20, and 30 nm singly charged particles are 50, 65, and 85 nm. The details of the fitting procedure can be found in the Supplement. While the model is a somewhat imprecise tool, it gives a qualitative picture of which size of ambient particles made up the bulk of the mass sampled for each collection. Representing the data as ion fractions also has the benefit of reducing the impact of sample matrix effects. For example, laboratory experiments

ACPD
14, 2087–2111, 2014

have indicated that the TDCIMS sensitivity to weak acids can be higher in the presence of higher concentrations of stronger acids.

Just prior to the campaign, the TDCIMS was modified to improve chemical specificity via the replacement of the quadrupole mass spectrometer with a high resolution time-of-flight mass spectrometer (HTOF; TofWerk AG). Associated with that modification, the vacuum chamber and ion optics were redesigned to interface the atmospheric pressure ion source with the HTOF. Several observations, both during the campaign and after post-campaign instrument modifications, suggest that the initial designs of the vacuum chamber and ion optics resulted in poor ion tranmission and excessive collisional dissociation of analyte ions. This had the effect of low sensitivity for positive ions in general and, we suspect, for organic species during these measurements.

A chemical calibration of the TDCIMS was performed on 30 May 2011 using ammonium sulfate aerosol generated by a nebulizer. This resulted in clear SO_2^- and SO_4^- signals in the negative ion spectrum. These ions likely result directly from the ionization of gas phase SO_2 or SO_3, suggesting that the very recalcitrant ammonium sulfate thermally decomposed on the wire rather than desorbing as a neutral salt. There was a negligible response in the positive ion spectrum to the ammonium sulfate calibration aerosol; however, ammonium was detected in some ambient mass spectra. Later laboratory measurements indicated that ammonium nitrate was detected as NO_2^- in the negative ion spectrum. Some organic nitrates would likely appear as NO_2^- as well. The instrument is roughly 100× more sensitive to ammonium nitrate (as NO_2^-) than to ammonium sulfate (as SO_2^-), based on laboratory calibrations.

2.3 HTDMA instrument

Aerosol growth factors were measured at Mace Head using the Manchester custom-built Hygroscopicity Tandem Differential Mobility Analyser (HTDMA; Duplissy et al., 2009). The growth factor (GF) is defined here as the ratio between the aerosol's equilibrium diameter at 90 % relative humidity (RH) and its dry diameter (< 15 % RH). To

ACPD
14, 2087–2111, 2014

measure this, the sample was drawn first through a membrane drier, to bring the RH down to < 15 %, then through a charge neutraliser. The first DMA was then used to select a particle size. This quasi-monodisperse aerosol sample was humidified at 90 % RH before being passed into a chamber where the temperature was maintained at 2–3 °C below the first DMA, for a residence time of around 10 s. A second DMA was then used to size scan the humidified aerosol, with particle detection provided by a water-based CPC (TSI model 3782), resulting in a GF distribution as a function of dry diameter (GF(D_0)). The raw data were inverted using the TDMAinv software described by Gysel et al. (2009). The nominal resolution of the instrument is 0.05 in GF space. The aerosol dry diameters selected during this campaign were 51, 75, 109, 162 and 258 nm, and GF was scanned between 0.8 and 2.8. The sizes most relevant for comparison to the TDCIMS data are 51 and 75 nm. The sample flow rate was maintained at 0.45 LPM, and the DMA sheath flows at 4.5 LPM.

Full descriptions of the calibrations needed for HTDMA measurements is given by Good et al. (2010). Briefly, dry scans (no humidification, RH < 15 %) were performed on a weekly basis in order to correct for the system transfer function, and for any offset between the DMAs. A size calibration of the first DMA was also performed at the start of measurements using latex spheres of a known size. In addition, a salt calibration was performed at the start and end of measurements, whereby an inorganic salt solution (typically ammonium sulphate or sodium chloride) was nebulised and sampled by the HTDMA at a set dry size of 150 nm. The RH was then scanned over a range of values to produce a humidogram (mean GF as a function of RH), which can be compared to modelled values from the Aerosol Diameter Dependent Equilibrium Mixing Model (ADDEM) (Topping et al., 2005).

ACPD
14, 2087–2111, 2014

3 Results

3.1 Background particles and events

Typical sub-micron background particle size distributions showed two main modes, an accumulation mode with a number peak around 200 nm and an Aitken mode with a number peak around 50–60 nm (Fig. 1). Typical total integrated aerosol number concentration was on the order of 500 cm^{-3}. There were also periods of up to a few hours during which background aerosol concentration was low, roughly 200–300 cm^{-3}. The lowest recorded concentration was ~ 100 cm^{-3}.

On several occasions lasting from hours to about two days, there were large increases in the concentrations of 10–60 nm particles (Fig. 1). The total particle number during these "nanoparticle enhancement events" was typically 1000–2000 cm^{-3}. During these events, there were also less pronounced but clear increases in particle number at sizes smaller than the main enhancement band, sometimes down to the roughly 4 nm cutoff size of the instrument. The enhancement events were primarily associated with polar air masses advected over the ocean and were very similar to the apparent open ocean particle production described by O'Dowd et al. (2010). Apparent coastal nucleation events also occurred, during which there were large, brief increases in < 10 nm particles. These coastal nucleation particles were too small to be analyzed with either the TDCIMS or the HTDMA, and we do not comment further on them in this work. The nanoparticle enhancement events referred to in the rest of this work pertain to the periods of strong 10–60 nm number concentration enhancement.

3.2 HTDMA observations

The HTDMA size bin closest to the sizes measured by the TDCIMS was at 51 nm dry mobility diameter. It is worth noting that the particle number enhancements during the events sometimes included 50–60 nm diameter particles and sometimes were confined to smaller sizes. For most of the measurement period, there were two distinct growth

ACPD
14, 2087–2111, 2014

factor (GF) modes, one around 1.5–1.7 and one around 2–2.3 (Fig. 3). The higher growth factor mode corresponds to highly hygroscopic sea salt, potentially at different degrees of aging. The lower GF mode could contain ammonium sulfate or some mixture of inorganic and organic components (Sjogren et al., 2007; Hersey et al., 2009). For larger marine particles measured in the eastern Atlantic, a GF of about 1.7 was attributed to internally mixed sulfate, ammonium, and organic particles (Allan et al., 2009).

We identified four characteristic particle distributions based on the SMPS and HTDMA observations, and averaged the HTDMA data over these periods. These were (1) non-event periods (background), (2) events with major enhancements only for particles smaller than 50 nm (sub-50 nm events), (3) events in which the number enhancements included 50 nm or greater particles (50 nm events), and (4) a period dominated by one high hygroscopicity mode (sea salt or SS). Examples of the different period types are shown in Fig. 1. During background conditions and sub-50 nm event conditions, both the 1.5–1.7 and 2–2.3 GF modes tended to be present. However, during events in which there were large enhancements in >50 nm particles, the highly hygroscopic mode decreased sharply and the 1.5–1.7 GF mode became larger (Fig. 3).

The mean distributions of the different periods suggest a progression of marine aerosol states, controlled in part by the nanoparticle enhancement events. During the "sea salt" period, only a high hygroscopicity mode was observed (GF ~ 2.3), and the mean GF was larger than for any other period. This period appears to have been dominated by relatively fresh sea salt in the size range above 50 nm. In the 50 nm event periods, there was a great abundance of GF 1.5–1.7 particles, and the GF 2–2.3 mode was almost eliminated. The elimination of the sea salt mode suggests either that the sea salt which had been present was significantly modified by the events, or that events occurred under conditions of lower sea salt loading. The new GF 1.5–1.7 particles seem likely to be sulfate particles with varying degrees of organic components, as ammonium sulfate has a growth factor of 1.7, and measured organic GFs are uniformly lower (Peng et al., 2001; Zardini et al., 2008; Hansson et al., 1998). Further

ACPD
14, 2087–2111, 2014

evidence that sulfate was involved is found in the TDCIMS observations (below). The "background" aerosol state may represent the aftermath of this process, in which the low GF mode has shifted still lower by addition of organics, and the high GF mode has returned (due to direct sea salt emission and/or uptake of inorganic acids). In this context, the second half of the "sea salt" period appears to represent the aftermath of an event that occurred elsewhere (Fig. 1). A strong enhancement of particle number was evident in the 20–40 nm range, but no growth from smaller sizes was observed, and the high GFs for all the observed HTDMA sizes (50 nm and greater) indicate that the sea salt present was not significantly modified by the addition of organic vapors.

3.3 TDCIMS observations

The size of particles sampled by the TDCIMS is dependent on the ambient size distribution, the selected RDMA voltage, and instrument characteristics such as charging efficiency and collection efficiency. The result in the case of these observations is that a fairly wide range of sizes was sampled during most particle collections. Therefore individual spectra may represent a variety of aerosol types, e.g. very small sulfate-dominated particles mixed with somewhat larger seasalt particles. Because the volume and mass go as the cube of the particle diameter, the sampled particle volume is typically skewed towards larger sizes. An estimate of collected particle volume by particle size is plotted, along with the volume mean diameter for collected particles (Fig. 1).

3.3.1 Negative ions

The negative ion spectra were dominated by Cl^-, SO_2^-, NO_2^-, and SO_4^-. A subset of the time series is plotted in Fig. 2 as fraction of total ion signal above detection for each mass spectrum. The observed Cl^- generally covaried with Na^+ and a $ClNa_2^+$ cluster in the positive ion spectrum, indicating the presence of sea salt. SO_2^- and SO_4^- are indicators of sulfate (SO_4^{2-}) in the particles. NO_2^- is an indicator of nitrate (NO_3^-) in the particles, potentially inorganic or organic in origin. Laboratory calibrations conducted

ACPD
14, 2087–2111, 2014

after the observations showed that the instrument is roughly 100× more sensitive to ammonium nitrate than to ammonium sulfate, so the relative nitrate concentrations in the particles are likely much lower than suggested by the relative ion abundances. Nitrate can also be prominent in the background signals, causing the occasional determination of negative particulate nitrate signals. Br^- was also occasionally measured at detectable levels, and it closely tracked Cl^-. I^- was not present at detectable levels.

The chloride to sulfate ratio (Cl^- to SO_2^- signal) was a useful diagnostic for characterizing the collected particles. For example, there was an event with an extremely high sulfate fraction (about 60 × Cl^-) on 26 May, most likely a volcanic plume resulting from the Grímsvötn volcano eruptions of 22–25 May. Air masses during this day came almost directly from the north near Iceland. During the seasalt period, the chloride to sulfate ratio was maintained at a relatively high level of about 3. Nonetheless, a significant sulfate fraction was still present despite the lack of a strong GF 1.5–1.7 mode in the HTDMA data during this period. Chloride to sulfate was generally lower during the long > 50 nm event that began on the 24th and during the period beginning on the 28th when the smallest particles and lowest particle volumes were collected. Brief intense sea spray bursts which occurred early in the campaign yielded chloride to sulfate ratios closer to 10, so this value is probably more indicative of fresh sea salt with a minor non-sea-salt sulfate (nss-sulfate) component. Chloride is about 17 times more abundant on a molar basis than sulfate in seawater (e.g. Savoie et al., 1989), so the TDCIMS sensitivity to sulfate was likely slightly higher than to chloride. Typical chloride to sulfate ion ratios were about 1–3. This ratio indicates that most of the observed sulfate was nss-sulfate.

3.3.2 Positive ions

The positive ion spectra were dominated by $(H_2O)Na^+$. Na^+ tracked the $(H_2O)Na^+$ signal but was smaller due to ion clustering in the instrument. The absolute sodium signal generally followed the chloride signal. Acetaldehyde, measured as $C_2H_5O^+$, was the only organic species which was regularly observed. It was not enhanced during the par-

ACPD
14, 2087–2111, 2014

ticle events. Acetaldehyde has a high saturation vapor pressure and is therefore most likely a fragmentation product of larger organic compounds. There were occasional instances when another organic species was found to be above the detection limit, and these are plotted as "Organics" in Fig. 1. These include $C_4H_9^+$, $CH_3O_2^+$, and $C_3H_7O^+$, but points above detection were rare, despite the fact that these species occasionally represented large relative ion fractions. Ion peaks which were above detection but not identified are plotted as "Others".

There were very few points for which NH_4^+ was above detection, making it difficult to discern patterns. The TDCIMS sensitivity to ammonium was clearly very low for this campaign (see Sect. 2). However, ammonium reached its highest fractional abundance during the apparent volcanic plume event on 26 May when a large amount of mass was collected and sulfate levels were high.

3.3.3 Characterizing collected particles

Correlation coefficients between estimated mass collected and TDCIMS signals were calculated for each of the major ions observed (Fig. 4). The data used are from the one-week time series presented in Fig. 3, including all characteristic periods, with the large outliers from the volcanic plume removed (three points removed for each ion). Sulfate signal (measured as SO_2^-) was the best explainer of collected mass ($r^2 = 0.36$). The amount of particle volume collected was primarily dependent on the presence or absence of nanoparticle enhancement events, so the event particles in general contained a significant sulfate fraction. Chloride and sodium had lower r^2 values of 0.15 and 0.14, and NO_2^- and $C_2H_5O^+$ had the least explanatory power for collected mass with r^2 values of 0.09 and 0.08. However, volume-normalized sulfate (sulfate ions per collected particle volume) was not generally higher during the events than at other times. This could be because the background particles are similar to the event particles, or because event particles contained more species that were not effectively detected by the TDCIMS, such as ammonium and organics. Other than for the sea salt period, there was not a clear distinction in TDCIMS-derived compositions among the various char-

ACPD
14, 2087–2111, 2014

acteristic periods. This observation, and the fact that there were typically two similar hygroscopicity modes throughout the measurements, suggests that the background, < 50 nm event, and 50 nm event particles had similar compositions with respect to the major ions observed.

3.4 Discussion

The frequent nanoparticle enhancement events observed at this site appear to stem from nucleation and subsequent growth by sulfate and potentially additional organic vapors. The increases in particle mass were at least partly due to sulfate, and the hygroscopicity measurements support the idea that sulfate is a major component of the event aerosol. The smaller but still clear increases in the number of very small (sub-10 nm) particles during the enhancement events also argues that the particles have grown from very small sizes. Given that the air came on an ocean trajectory via the Arctic and North Atlantic Oceans, the sulfur source is most likely biological (i.e. dimethyl sulfide). The event periods can be quite long (over a day), and the lifetime of such small particles is generally quite short (a few hours). The mechanisms that generate these particles appear therefore to operate both in the day and the night.

Our observations support the idea that sea salt is a major component of marine aerosol even at very small sizes. Sodium and chloride were observed in essentially all collected particle samples, but neither species was as strongly linked to the nanoparticle enhancement events as was sulfate. During the events, the sea salt particles may have taken up organic vapors which contributed to the particle volume during the events and resulted in a decrease in their hygroscopicity. Whether the sea salt particles transitioned into the 1.5–1.7 GF hygroscopicity mode during the events is not clear from these observations. In general we appear to have observed the progression of fresh sea salt to more aged, less hygroscopic forms.

ACPD
14, 2087–2111, 2014

4 Conclusions

The chemical composition and hygroscopicity of marine nanoparticles were measured during May 2011 at the coastal site Mace Head. There was essentially always a sea salt component in the observered aerosol, at different stages of aging. There were several events during which the number concentrations of 10–60 nm particles increased dramatically. These events appear to involve the nucleation of new particles over the ocean, and these recently grown particles contain a significant sulfate fraction. The similarity between the characteristics of event particles and background particles and the frequency of the events suggest that these events are a major source of nanoparticles in this marine environment.

Supplementary material related to this article is available online at http://www.atmos-chem-phys-discuss.net/14/2087/2014/acpd-14-2087-2014-supplement.pdf.

Acknowledgements. This work was supported by the the European Aerosols, Clouds, and Trace gases Research InfraStructure (ACTRIS) Network, the Saastamoinen Foundation, US DOE Grant DE-SC0006861, and US NSF Grant 0919317. The National Center for Atmospheric Research is supported by NSF. Thanks to Ru-Jin Huang for comments on the manuscript.

References

Allan, J. D.: Submicron aerosol composition at Trinidad Head, California, during ITCT 2K2: its relationship with gas phase volatile organic carbon and assessment of instrument performance, J. Geophys. Res., 109, D23S24, doi:10.1029/2003JD004208, 2004. 2090

Allan, J. D., Topping, D. O., Good, N., Irwin, M., Flynn, M., Williams, P. I., Coe, H., Baker, A. R., Martino, M., Niedermeier, N., Wiedensohler, A., Lehmann, S., Müller, K., Herrmann, H., and McFiggans, G.: Composition and properties of atmospheric particles in the eastern

ACPD
14, 2087–2111, 2014

Atlantic and impacts on gas phase uptake rates, Atmos. Chem. Phys., 9, 9299–9314, doi:10.5194/acp-9-9299-2009, 2009. 2097
Bzdek, B. R., Zordan, C. A., Luther, G. W., and Johnston, M. V.: Nanoparticle chemical composition during new particle formation, Aerosol Sci. Tech., 45, 1041–1048, doi:10.1080/02786826.2011.580392, 2011. 2089
Bzdek, B. R., Zordan, C. A., Pennington, M. R., Luther, G. W., and Johnston, M. V.: Quantitative assessment of the sulfuric acid contribution to new particle growth., Environ. Sci. Technol., 46, 4365–4373, doi:10.1021/es204556c, 2012.2089
Chen, D.-R. and Pui, D.: A high efficiency, high throughput unipolar aerosol charger for nanoparticles, J. Nanopart. Res., 1, 115–126, 1999. 2091
Clarke, A., Kapustin, V., Howell, S., Moore, K., Lienert, B., Masonis, S., Anderson, T., and Covert, D.: Sea-salt size distributions from breaking waves: implications for marine aerosol production and optical extinction measurements during SEAS*, J. Atmos. Ocean. Tech., 20, 1362–1374, doi:10.1175/1520-0426(2003)020<1362:SSDFBW>2.0.CO;2, 2003. 2090
Clarke, A. D., Owens, S. R., and Zhou, J.: An ultrafine sea-salt flux from breaking waves: implications for cloud condensation nuclei in the remote marine atmosphere, J. Geophys. Res., 111, 1–14, doi:10.1029/2005JD006565, 2006. 2090
Dall'Osto, M., Monahan, C., Greaney, R., Beddows, D. C. S., Harrison, R. M., Ceburnis, D., and O'Dowd, C. D.: A statistical analysis of North East Atlantic (submicron) aerosol size distributions, Atmos. Chem. Phys., 11, 12567–12578, doi:10.5194/acp-11-12567-2011, 2011. 2090
Donahue, N. M., Trump, E. R., Pierce, J. R., and Riipinen, I.: Theoretical constraints on pure vapor-pressure driven condensation of organics to ultrafine particles, Geophys. Res. Lett., 38, L16801, doi:10.1029/2011GL048115, 2011. 2089
Draxler, R. and Hess, G.: Description of the HYSPLIT_4 modeling system, NOAA Tech. Memo ERL ARL-224, Tech. rep., NOAA Air Resources Laboratory, Silver Spring, MD, 1997. 2091
Duplissy, J., Gysel, M., Sjogren, S., Meyer, N., Good, N., Kammermann, L., Michaud, V., Weigel, R., Martins dos Santos, S., Gruening, C., Villani, P., Laj, P., Sellegri, K., Metzger, A., McFiggans, G. B., Wehrle, G., Richter, R., Dommen, J., Ristovski, Z., Baltensperger, U., and Weingartner, E.: Intercomparison study of six HTDMAs: results and recommendations, Atmos. Meas. Tech., 2, 363–378, doi:10.5194/amt-2-363-2009, 2009. 2094
Eisele, F. L. and McMurry, P. H.: Recent progress in understanding particle nucleation and growth, Philos. T. R. Soc. B, 352, 191–201, doi:10.1098/rstb.1997.0014, 1997. 2089

ACPD
14, 2087–2111, 2014

Good, N., Coe, H., and McFiggans, G.: Instrumentational operation and analytical methodology for the reconciliation of aerosol water uptake under sub- and supersaturated conditions, Atmos. Meas. Tech., 3, 1241–1254, doi:10.5194/amt-3-1241-2010, 2010. 2095

Gysel, M., McFiggans, G., and Coe, H.: Inversion of tandem differential mobility analyser (TDMA) measurements, J. Aerosol Sci., 40, 134–151, doi:10.1016/j.jaerosci.2008.07.013, 2009. 2095

Hansson, H., Rood, M., Koloutsou-Vakakis, S., Hämeri, K., Orsini, D., and Wiedensohler, A.: NaCl aerosol particle hygroscopicity dependence on mixing with organic compounds, J. Atmos. Chem., 31, 321–346, doi:10.1023/A:1006174514022, 1998. 2097

Heintzenberg, J., Covert, D. C., and Van Dingenen, R.: Size distribution and chemical composition of marine aerosols: a compilation and review, Tellus B, 52, 1104–1122, doi:10.1034/j.1600-0889.2000.00136.x, 2000. 2089, 2090

Hersey, S. P., Sorooshian, A., Murphy, S. M., Flagan, R. C., and Seinfeld, J. H.: Aerosol hygroscopicity in the marine atmosphere: a closure study using high-time-resolution, multiple-RH DASH-SP and size-resolved C-ToF-AMS data, Atmos. Chem. Phys., 9, 2543–2554, doi:10.5194/acp-9-2543-2009, 2009. 2097

Hoppel, W. A., Frick, G. M., and Fitzgerald, J. W.: Deducing droplet concentration and supersaturation in marine boundary layer clouds from surface aerosol measurements, J. Geophys. Res., 101, 26553, doi:10.1029/96JD02243, 1996. 2089

Khvorostyanov, V. I. and Curry, J. A.: Refinements to the Köhler's theory of aerosol equilibrium radii, size spectra, and droplet activation: effects of humidity and insoluble fraction, J. Geophys. Res., 112, D05206, doi:10.1029/2006JD007672, 2007. 2089

Kuang, C., McMurry, P. H., McCormick, A. V., and Eisele, F. L.: Dependence of nucleation rates on sulfuric acid vapor concentration in diverse atmospheric locations, J. Geophys. Res., 113, 1–9, doi:10.1029/2007JD009253, 2008. 2089

Kuang, C., Chen, M., Zhao, J., Smith, J., McMurry, P. H., and Wang, J.: Size and time-resolved growth rate measurements of 1 to 5 nm freshly formed atmospheric nuclei, Atmos. Chem. Phys., 12, 3573–3589, doi:10.5194/acp-12-3573-2012, 2012. 2089

Kulmala, M., Vehkamäki, H., Petäjä, T., Dal Maso, M., Lauri, A., Kerminen, V.-M., Birmili, W., and McMurry, P.: Formation and growth rates of ultrafine atmospheric particles: a review of observations, J. Aerosol Sci., 35, 143–176, doi:10.1016/j.jaerosci.2003.10.003, 2004. 2088

ACPD
14, 2087–2111, 2014

Mäkelä, J. M.: Biogenic iodine emissions and identification of end-products in coastal ultrafine particles during nucleation bursts, J. Geophys. Res., 107, 8110, doi:10.1029/2001JD000580, 2002. 2089

McFiggans, G., Bale, C. S. E., Ball, S. M., Beames, J. M., Bloss, W. J., Carpenter, L. J., Dorsey, J., Dunk, R., Flynn, M. J., Furneaux, K. L., Gallagher, M. W., Heard, D. E., Hollingsworth, A. M., Hornsby, K., Ingham, T., Jones, C. E., Jones, R. L., Kramer, L. J., Langridge, J. M., Leblanc, C., LeCrane, J.-P., Lee, J. D., Leigh, R. J., Longley, I., Mahajan, A. S., Monks, P. S., Oetjen, H., Orr-Ewing, A. J., Plane, J. M. C., Potin, P., Shillings, A. J. L., Thomas, F., von Glasow, R., Wada, R., Whalley, L. K., and Whitehead, J. D.: Iodine-mediated coastal particle formation: an overview of the Reactive Halogens in the Marine Boundary Layer (RHaMBLe) Roscoff coastal study, Atmos. Chem. Phys., 10, 2975–2999, doi:10.5194/acp-10-2975-2010, 2010. 2089

Mcinnes, L., Covert, D., and Baker, B.: The number of sea-salt, sulfate, and carbonaceous particles in the marine atmopshere: EM Measurements consistent with the ambient size distribution, Tellus B, 49, 303–313, doi:10.1034/j.1600-0889.49.issue3.6.x, 1997. 2090

McMurry, P., Ghimire, A., Ahn, H.-K., Sakurai, H., Moore, K., Stolzenburg, M., and Smith, J.: Sampling nanoparticles for chemical analysis by low resolution electrical mobility classification, Environ. Sci. Technol., 43, 4653–4658, doi:10.1021/es8029335, 2009. 2091, 2093

McMurry, P. H.: New particle formation in the presence of an aerosol: rates, time scales, and sub-0.01 µm size distributions, J. Colloid Interf. Sci., 95, 72–80, 1983. 2090

O'Dowd, C., Monahan, C., and Dall'Osto, M.: On the occurrence of open ocean particle production and growth events, Geophys. Res. Lett., 37, L19805, doi:10.1029/2010GL044679, 2010. 2090, 2096

O'Dowd, C. D. and Hoffmann, T.: Coastal new particle formation: a review of the current state-of-the-art, Environ. Chem., 2, 245, doi:10.1071/EN05077, 2005. 2089

Peng, C., Chan, M. N., and Chan, C. K.: The hygroscopic properties of dicarboxylic and multifunctional acids: measurements and UNIFAC predictions., Environ. Sci. Technol., 35, 4495–4501, 2001. 2097

Pierce, J. R. and Adams, P. J.: Global evaluation of CCN formation by direct emission of sea salt and growth of ultrafine sea salt, J. Geophys. Res., 111, D06203, doi:10.1029/2005JD006186, 2006.2089

Russell, L. M. and Singh, E. G.: Submicron salt particle production in bubble bursting, Aerosol Sci. Tech., 40, 664–671, doi:10.1080/02786820600793951, 2006. 2090

ACPD
14, 2087–2111, 2014

Savoie, D., Prospero, J., and Saltzman, E.: Non-sea-salt sulfate and nitrate in trade wind aerosols at Barbados: evidence for long-range transport, J. Geophys. Res., 94, 5069–5080, 1989. 2099

Seinfeld, J. H. and Pandis, S. N.: Atmospheric Chemistry and Physics: from Air Pollution to Climate Change, Wiley-Interscience, Hoboken, NJ, USA, 1997. 2089

Sjogren, S., Gysel, M., Weingartner, E., Baltensperger, U., Cubison, M., Coe, H., Zardini, A. A., Marcolli, C., Krieger, U., and Peter, T.: Hygroscopic growth and water uptake kinetics of two-phase aerosol particles consisting of ammonium sulfate, adipic and humic acid mixtures, J. Aerosol Sci., 38, 157–171, doi:10.1016/j.jaerosci.2006.11.005, 2007. 2097

Smith, J. N. and Rathbone, G. J.: Carboxylic acid characterization in nanoparticles by thermal desorption chemical ionization mass spectrometry, Int. J. Mass Spectrom., 274, 8–13, doi:10.1016/j.ijms.2008.04.008, 2008. 2092

Smith, J. N., Moore, K. F., McMurry, P. H., and Eisele, F. L.: Atmospheric measurements of sub-20 nm diameter particle chemical composition by thermal desorption chemical ionization mass spectrometry, Aerosol Sci. Tech., 38, 100–110, doi:10.1080/02786820490249036, 2004. 2091

Solomon, S., Qin, D., Manning, M., Chen, Z., Marquis, M., Averyt, K., Tignor, M., and Miller, H.: IPCC 2007: Climate Change 2007: The Physical Science Basis, Contribution of Working Group I to the Fourth Assessment Report of the Intergovernmental Panel on Climate Change, Tech. rep., Cambridge University Press, Cambridge, 2007. 2088

Spracklen, D. V., Carslaw, K. S., Kulmala, M., Kerminen, V.-M., Mann, G. W., and Sihto, S.-L.: The contribution of boundary layer nucleation events to total particle concentrations on regional and global scales, Atmos. Chem. Phys., 6, 5631–5648, doi:10.5194/acp-6-5631-2006, 2006. 2088

Spracklen, D. V., Carslaw, K. S., Merikanto, J., Mann, G. W., Reddington, C. L., Pickering, S., Ogren, J. A., Andrews, E., Baltensperger, U., Weingartner, E., Boy, M., Kulmala, M., Laakso, L., Lihavainen, H., Kivekäs, N., Komppula, M., Mihalopoulos, N., Kouvarakis, G., Jennings, S. G., O'Dowd, C., Birmili, W., Wiedensohler, A., Weller, R., Gras, J., Laj, P., Sellegri, K., Bonn, B., Krejci, R., Laaksonen, A., Hamed, A., Minikin, A., Harrison, R. M., Talbot, R., and Sun, J.: Explaining global surface aerosol number concentrations in terms of primary emissions and particle formation, Atmos. Chem. Phys., 10, 4775–4793, doi:10.5194/acp-10-4775-2010, 2010. 2089

ACPD
14, 2087–2111, 2014

Topping, D. O., McFiggans, G. B., and Coe, H.: A curved multi-component aerosol hygroscopicity model framework: Part 1 – Inorganic compounds, Atmos. Chem. Phys., 5, 1205–1222, doi:10.5194/acp-5-1205-2005, 2005. 2095

Voisin, D., Smith, J., Sakurai, H., McMurry, P., and Eisele, F.: Thermal desorption chemical ionization mass spectrometer for ultrafine particle chemical composition, Aerosol Sci. Tech., 37, 471–475, doi:10.1080/02786820390125232, 2003. 2091

Wang, M. and Penner, J. E.: Aerosol indirect forcing in a global model with particle nucleation, Atmos. Chem. Phys., 9, 239–260, doi:10.5194/acp-9-239-2009, 2009. 2088

Whitehead, J. D., McFiggans, G. B., Gallagher, M. W., and Flynn, M. J.: Direct linkage between tidally driven coastal ozone deposition fluxes, particle emission fluxes, and subsequent CCN formation, Geophys. Res. Lett., 36, L04806, doi:10.1029/2008GL035969, 2009. 2089

Whitehead, J. D., McFiggans, G., Gallagher, M. W., and Flynn, M. J.: Simultaneous coastal measurements of ozone deposition fluxes and iodine-mediated particle emission fluxes with subsequent CCN formation, Atmos. Chem. Phys., 10, 255–266, doi:10.5194/acp-10-255-2010, 2010. 2089

Yu, F. and Luo, G.: Simulation of particle size distribution with a global aerosol model: contribution of nucleation to aerosol and CCN number concentrations, Atmos. Chem. Phys., 9, 7691–7710, doi:10.5194/acp-9-7691-2009, 2009. 2088

Zardini, A. A., Sjogren, S., Marcolli, C., Krieger, U. K., Gysel, M., Weingartner, E., Baltensperger, U., and Peter, T.: A combined particle trap/HTDMA hygroscopicity study of mixed inorganic/organic aerosol particles, Atmos. Chem. Phys., 8, 5589–5601, doi:10.5194/acp-8-5589-2008, 2008. 2097

Zhang, R., Khalizov, A., Wang, L., Hu, M., and Xu, W.: Nucleation and growth of nanoparticles in the atmosphere., Chem. Rev., 112, 1957–2011, doi:10.1021/cr2001756, 2012. 2089

Zhang, S.-H., Akutsu, Y., Russell, L. M., Flagan, R. C., and Seinfeld, J. H.: Radial differential mobility analyzer, Aerosol Sci. Tech., 12, 357–372, doi:10.1080/02786829508965320, 1995. 2091

ACPD
14, 2087–2111, 2014

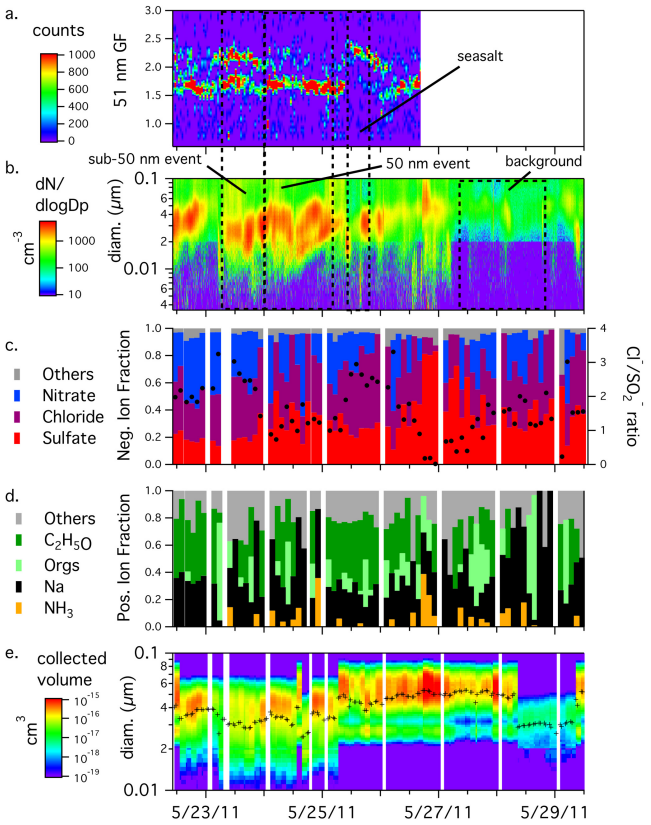

Fig. 1. (a) Hygroscopic growth factor for 51 nm dry diameter particles. **(b)** Ambient particle size distribution. **(c)** Fracitonal ion abundance for negative spectra and Cl^- to SO_2^- signal ratio (black points). **(d)** Fractional ion abundance for positive spectra. **(e)** Estimated volume of collected aerosol in each size bin (cm^{-3}) and volume mean diameter for each collection (black crosses).

ACPD
14, 2087–2111, 2014

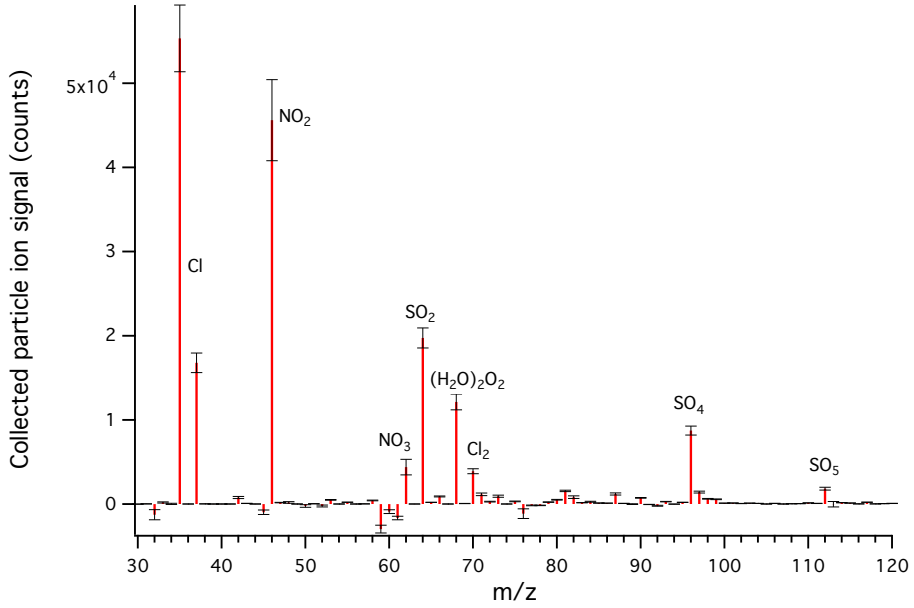

Fig. 2. Campaign-averaged mass spectrum of particle composition in negative ion mode, measured by TDCIMS. This is an average of background-corrected points, and one standard error bars are plotted.

ACPD
14, 2087–2111, 2014

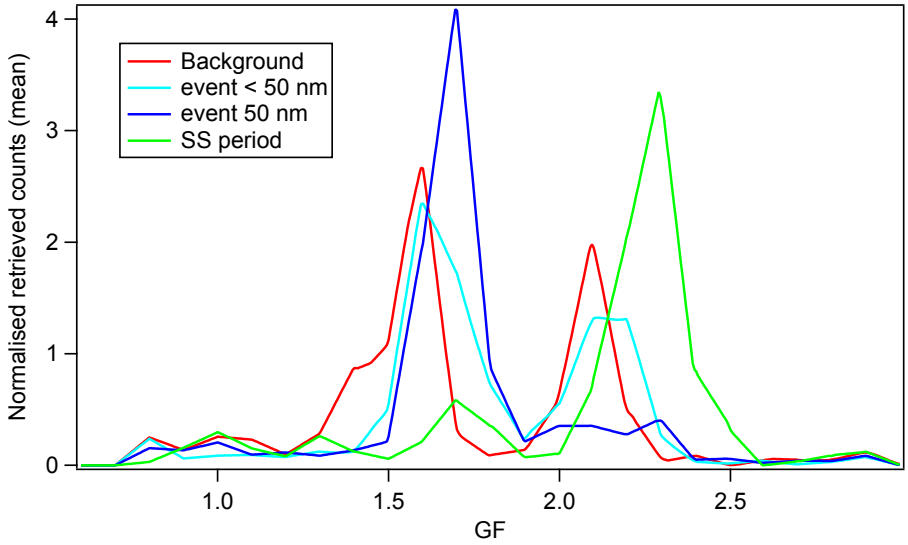

Fig. 3. Averaged HTDMA growth factor (GF) distributions for 51 nm dry diameter particles for the four characteristic periods during the observations. There were usually two main modes, a seasalt mode with GF > 2, and a GF 1.5–1.7 mode which was probably dominated by sulfate.

ACPD
14, 2087–2111, 2014

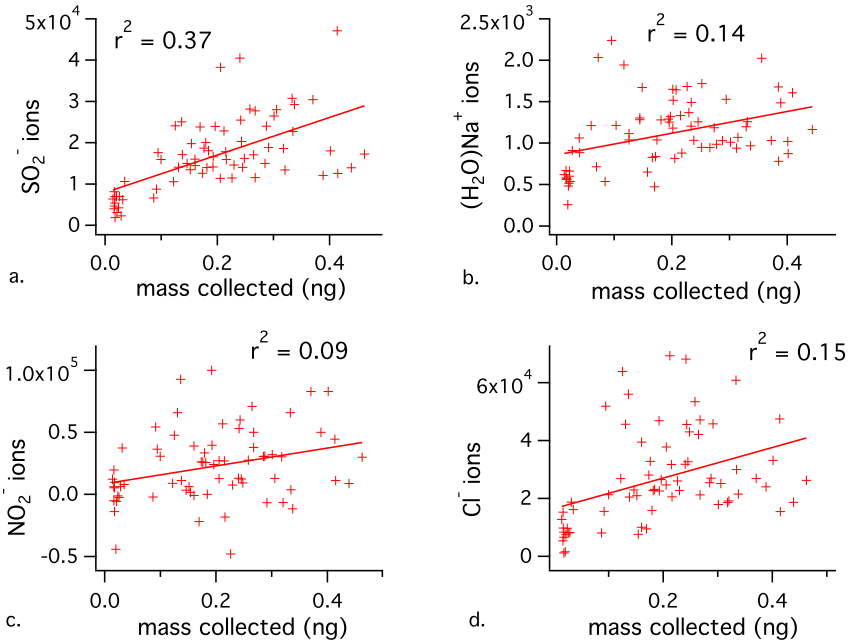

Fig. 4. Correlations between individual species measured by TDCIMS and total estimated collected mass for the period shown in Fig. 1. Three points prior to midnight on the 26th were excluded, due to very high sulfate levels attributed to a volcanic plume. All linear slopes are greater than two standard deviations above zero. SO_2^-, an indicator of particle sulfate, is the best explainor of particle mass collected by the instrument.

ACPD
14, 2087–2111, 2014